PHYSICAL REVIEW D **95,** 074018 (2017)

# Higher hybrid bottomonia in an extended potential model

Nosheen Akbar,[*] M. Atif Sultan,[†] Bilal Masud,[‡] and Faisal Akram[§]

*COMSATS Institute of Information and Technology, Lahore 54000, Pakistan*
*and Centre For High Energy Physics, University of the Punjab, Lahore 54590, Pakistan*

(Received 19 December 2015; published 13 April 2017)

Using our extension of the quark potential model to hybrid mesons that fits well with the available lattice results, we now calculate the masses, radii, wave functions at the origin, leptonic and two-photon decay widths, and $E1$ and $M1$ radiative transitions for a significant number of bottomonium mesons. These mesons include both conventional and hybrid ones with radial and angular excitations. Our numerical solutions of the Schrödinger equation are related to QCD through the Born-Oppenheimer approach. Relativistic corrections in masses and decay widths are also calculated by applying the leading-order perturbation theory. The calculated results are compared with available experimental data and the theoretical results by other groups. We also identify the states of $\Upsilon(10860)$, $\Upsilon(11020)$, and $Y_b(10890)$ mesons by comparing their experimental masses and decay widths to our results.

DOI: 10.1103/PhysRevD.95.074018

## I. INTRODUCTION

Models of QCD can be tested by numerical (lattice) simulations of QCD or by hard experiments. Earlier, we suggested extensions to gluonic excitations of the analytical expressions for the quark-antiquark potential [1]. We have good fits of the parameters in these expressions to the lattice simulations for the ground and *excited-state* gluonic field energy values available in Ref. [2] for discrete quark-antiquark separations. In Refs. [1,3], we used these expressions to calculate a number of measurable quantities for possible conventional and hybrid charmonia. Now, for the new sector of bottomonia, we provide a comprehensive list of phenomenological implications that can be obtained through solving the Schrödinger equation for our extended potential model; we report results for a variety of conventional and hybrid mesons. We include relativistic corrections and some other refinements to this nonrelativistic treatment. For relating the angular momenta in our model with experimentally reported parity $P$ and charge parity $C$, we use the flux tube model [4] that is applicable to hybrid quantum numbers as well. But the flux tube model was suggested only for large quark-antiquark separations; we pointed out earlier [1] that the additional potential term $(\frac{\pi}{r})$ for hybrids resulting from this model differs significantly from the actual lattice simulations performed [5]. Thus, instead of the flux tube model potential, we use our previously suggested quark potential model that has a very good comparison with these lattice-generated numbers. The relationship of the quark potential model to QCD obtained through the adiabatic approximation and the Born-Oppenheimer formalism applies to our extended potential model as well; the already-published [1,3,5,6] use of the Born-Oppenheimer approach in hadronic physics includes gluonic excitations. Using a potential model, we are able to calculate masses, root-mean-square radii, and radial wave functions at origin of ground state and radially excited hybrid mesons as well. The radial wave function at the origin is used in turn to calculate leptonic and two-photon decay widths, and radiative transitions of these mesonic states. A comparison of our results for bottomonium mesons of specified $J^{PC}$ states with experimentally known masses and decay widths with the same $J^{PC}$ can help in identifying quarks and gluonic field configurations of the observed bottomonium mesons like $\Upsilon(10860)$, $\Upsilon(11020)$, and $Y_b(10890)$.

Heavy hybrid mesons have also been studied using theoretical approaches like the constituent gluon model [7–9], QCD sum rule [10–17], lattice QCD [6], and Bethe-Salpeter equation [18]. Wherever possible, we compare with these theoretical results, along with available experimental numbers.

The paper is organized as follows. In Sec. II, the potential models used for conventional and hybrid mesons are written. Then, using these potential models, radial wave functions for the ground and excited states of conventional and hybrid bottomonium mesons are calculated by numerically solving the Schrödinger equation. The relativistic corrections are subsequently included by the perturbation theory. The formulas used to calculate leptonic and two-photon decay widths and radiative $E1$ and $M1$ transitions are also written in this section. Numerical results for these quantities for a variety of conventional and hybrid mesons are reported in Sec. III. Using our masses and leptonic decay widths for different $J^{PC}$ bottomonium states, we also suggest possible assignments of $\Upsilon(10860)$, $\Upsilon(11020)$, and

[*]nosheenakbar@ciitlahore.edu.pk
[†]atifsultan.chep@pu.edu.pk
[‡]bilalmasud.chep@pu.edu.pk
[§]faisal.chep@pu.edu.pk

 

$Y_b(10890)$ mesonic states indicated through our extension of the quark model to hybrids.

## II. CONVENTIONAL AND HYBRID BOTTOMONIUM MESONS

### A. Spectrum of conventional mesons

To study the spectrum of conventional bottomonium states, we used the semirelativistic Hamiltonian including the lowest-order relativistic correction,

$$H = 2m_b + \frac{p^2}{2\mu} - \left(\frac{1}{4m_b^3}\right)p^4 + V_{q\bar{q}}(r), \tag{1}$$

where $\mu = m_b/2$ is the reduced mass of the system and $m_b$ is the constituent mass of the bottom quark. The effective quark-antiquark potential $V_{q\bar{q}}(r)$ adopted from Ref. [19] carries Gaussian-smeared contact hyperfine interaction, one gluon exchange spin-orbit and tensor terms, and the long-ranged spin-orbit term in addition to the linear plus Coulombic terms. The complete expression of $V_{q\bar{q}}(r)$ is given by

$$V_{q\bar{q}}(r) = \frac{-4\alpha_s}{3r} + br + \frac{32\pi\alpha_s}{9m_b^2}\left(\frac{\sigma}{\sqrt{\pi}}\right)^3 e^{-\sigma^2 r^2}\mathbf{S}_b.\mathbf{S}_{\bar{b}} + \frac{1}{m_b^2}\left[\left(\frac{2\alpha_s}{r^3} - \frac{b}{2r}\right)\mathbf{L}.\mathbf{S} + \frac{4\alpha_s}{r^3}T\right]. \tag{2}$$

The Coulombic term which is proportional to strong coupling constant $\alpha_s$ arises from the one-gluon-exchange interaction dominating at short distance, whereas the linear term proportional to string tension $b$ is required to produce confinement in the system. The Gaussian-smeared contact hyperfine interaction proportional to $\mathbf{S}_b.\mathbf{S}_{\bar{b}}$ and the short-distance spin-orbit and the tensor interactions are also produced by the one-gluon-exchange process, whereas the long-ranged spin-orbit term is produced by the Lorentz scalar confinement. The tensor operator in the $|J, L, S\rangle$ basis is given by

$$T = \begin{cases} -\frac{1}{6(2L+3)}, & J = L+1 \\ +\frac{1}{6}, & J = L \\ -\frac{L+1}{6(2L-1)}, & J = L-1. \end{cases} \tag{3}$$

Here, $L$ and $S$ are quantum numbers of the relative orbital angular momentum of quark-antiquark and the total spin angular momentum of the system, respectively. The effective potentials defined above in Eq. (2) carries four unknown parameters, strong coupling constant $\alpha_s$, string tension $b$, width $\sigma$, and bottom quark constituent mass $m_b$. We fixed them by fitting the resulting spectrum to the experimental data composed of masses of ten well-known states of bottomonium mesons given in Table I. The best-fitted values of these parameters, with relativistic correction, were found to be $\alpha_s = 0.4$, $b = 0.11$ GeV$^2$, $\sigma = 1$ GeV, and $m_b = 4.89$ GeV. Without the relativistic corrections, the best-fitted values of parameters are $\alpha_s = 0.36$, $b = 0.1340$ GeV$^2$, $\sigma = 1.34$ GeV, and $m_b = 4.825$ GeV. To calculate the spectrum and the corresponding wave functions of the states of the $b\bar{b}$ system, we numerically solved the radial Schrödinger equation given by

$$U''(r) + 2\mu\left(E - V(r) - \frac{\langle L_{q\bar{q}}^2\rangle}{2\mu r^2}\right)U(r) = 0, \tag{4}$$

where $U(r) = rR(r)$ with $R(r)$ is the radial part of the wave function and $\langle L_{q\bar{q}}^2\rangle = L(L+1)$. Nontrivial solutions of this equation, existing only for certain discrete values of $E$, were found by the shooting method. The above Schrödinger equation assumes that the Hamiltonian $H = \frac{p^2}{2\mu} + V_{q\bar{q}}(r)$, i.e., without the constant term $2m_b$ and the relativistic correction. Thus, to obtain the mass of a $b\bar{b}$ state, we added the constituent quark masses to the above energy $E$, which was further corrected by the perturbation theory for the lowest-order relativistic correction to the Hamiltonian. That is,

$$m_{b\bar{b}} = 2m_b + E + \langle\Psi|\Delta H_{\rm rel}|\Psi\rangle, \tag{5}$$

where $\Delta H_{\rm rel} = -(\frac{1}{4m_b^3})p^4$ and $\Psi$ is the complete wave function of $b\bar{b}$ obtained by solving the above Schrödinger equation. It is noted that in the limit $r \to 0$ the potential $V_{q\bar{q}}(r) \sim \frac{2\alpha_s}{r^3}(\mathbf{L}.\mathbf{S} + 2T)$. It turns out that for $S = 1$, $\mathbf{L}.\mathbf{S} + 2T$ is negative for $J = L$ and $J = L - 1$. As a result, the potential becomes strongly attractive at short distance, and the resultant wave function becomes unstable in this limit. To circumvent this problem, we calculated the meson masses by solving the Schrödinger equation initially without the spin-orbit coupling. The effect of spin-orbit interaction was subsequently included through the leading-order perturbative correction to the meson mass. However, calculating the perturbative correction to the wave function is difficult, as in this case the contribution comes from all possible mass eigenstates. Therefore, in this case, we applied the smearing of position coordinates, as discussed in Ref. [4], to change the power behaviors of the potential at small distance. At small distance, smearing makes the potential less divergent than $1/r^2$. Thus, with its use, the repulsive centrifugal potential $l(l+1)/(2\mu r^2)$ remains dominating at small distance even if $\mathbf{L}.\mathbf{S} + 2T$ is negative.

### B. Characteristics of hybrid bottomonium mesons

Our study of the hybrid meson is based on the Born-Oppenheimer (BO) approximation in which energy levels of the gluonic field are first calculated in the presence of a static $q\bar{q}$ pair at fixed distance $r$ by Monte Carlo estimates

TABLE I. Masses; root-mean-square radii; and the radial wave function at the origin for ground, radial, and orbital excited states of bottomonium mesons. Our calculated masses are rounded to 0.0001 GeV.

| | Our calculated mass | | Theoretical mass | | Experimental mass | Our calculated | Others theor. | Our calculated |
|---|---|---|---|---|---|---|---|---|
| Meson | Relativistic [GeV] | NR [GeV] | Relativistic [20] potential model [GeV] | NR potential model [GeV] | [21] [GeV] | $\sqrt{\langle r^2\rangle}$ [fm] | calculated $\sqrt{\langle r^2\rangle}$ [22] [fm] | $\lvert R(0)\rvert^2$ [GeV$^3$] |
| $\eta_b(1^1S_0)$ | 9.4926 | 9.5079 | 9.402 | 9.448 [23], 9.428 [24] | $9.399 \pm 0.0023$ | 0.2265 | ⋯ | 11.8099 |
| $\Upsilon(1^3S_1)$ | 9.5098 | 9.5299 | 9.465 | 9.459 [23], 9.460 [24] | $9.4603 \pm 0.00026$ | 0.2328 | 0.23 | 11.4185 |
| $\eta_b(2^1S_0)$ | 10.0132 | 10.0041 | 9.976 | 10.006[23], 10.190 [24] | $9.999^{+2.8}_{-1.9}$ | 0.5408 | ⋯ | 4.0509 |
| $\Upsilon(2^3S_1)$ | 10.0169 | 10.0101 | 10.003 | 10.009[23], 10.219 [24] | $10.02326 \pm 0.00031$ | 0.5448 | 0.52 | 4.0393 |
| $\eta_b(3^1S_0)$ | 10.2792 | 10.2912 | 10.336 | 10.352 [23], 10.372 [24] | ⋯ | 0.8018 | ⋯ | 2.9327 |
| $\Upsilon(3^3S_1)$ | 10.2815 | 10.295 | 10.354 | 10.354 [23], 10.401 [24] | $10.3552 \pm 0.0005$ | 0.8047 | 0.78 | 2.9265 |
| $\eta_b(4^1S_0)$ | 10.4854 | 10.5214 | 10.623 | 10.473 [24] | ⋯ | 1.0273 | ⋯ | 2.4758 |
| $\Upsilon(4^3S_1)$ | 10.4872 | 10.5244 | 10.635 | 10.502 [24] | $10.5794 \pm 0.0012$ | 1.0296 | 1.02 | 2.4705 |
| $\eta_b(5^1S_0)$ | 10.6626 | 10.7226 | 10.869 | ⋯ | ⋯ | ⋯ | ⋯ | 2.2167 |
| $\Upsilon(5^3S_1)$ | 10.6642 | 10.7251 | 10.878 | ⋯ | | 1.2324 | 1.24 | 2.2120 |
| $\eta_b(6^1S_0)$ | 10.8219 | 10.9053 | 11.097 | ⋯ | ⋯ | ⋯ | ⋯ | 2.0452 |
| $\Upsilon(6^3S_1)$ | 10.8233 | 10.9074 | 11.102 | ⋯ | ⋯ | 1.4195 | 1.45 | 2.0408 |
| $\eta_b(7^1S_0)$ | 10.9686 | 11.0748 | | ⋯ | ⋯ | | | 1.9211 |
| $\Upsilon(7^3S_1)$ | 10.9698 | 11.0767 | | ⋯ | ⋯ | ⋯ | ⋯ | 1.9170 |
| $h_b(1^1P_1)$ | 9.9672 | 9.9279 | 9.882 | | $9.8993 \pm 0.0001$ | 0.4347 | ⋯ | 0 |
| $\chi_0(1^3P_0)$ | 9.8510 | 9.9232 | 9.847 | 9.871 [23], 10.1160 [24] | $9.85944 \pm 0.00042 \pm 0.00031$ | 0.4375 | ⋯ | 0 |
| $\chi_1(1^3P_1)$ | 9.9612 | 9.9295 | 9.876 | 9.897 [23], 10.190 [24] | $9.89278 \pm 0.00026 \pm 0.00031$ | 0.4379 | ⋯ | 0 |
| $\chi_2(1^3P_2)$ | 9.9826 | 9.9326 | 9.897 | 9.916 [23], 10.219 [24] | $9.91221 \pm 0.00026 \pm 0.00031$ | 0.4375 | 0.42 | 0 |
| $h_b(2^1P_1)$ | 10.2342 | 10.2213 | 10.250 | | ⋯ | 0.7114 | ⋯ | 0 |
| $\chi_0(2^3P_0)$ | 10.2098 | 10.2197 | 10.226 | 10.232 [23], 10.343 [24] | $10.2325 \pm 0.0004 \pm 0.0005$ | 0.7132 | ⋯ | 0 |
| $\chi_1(2^3P_1)$ | 10.2306 | 10.2232 | 10.246 | 10.255[23], 10.372 [24] | $10.25546 \pm 0.00022 \pm 0.00050$ | 0.7139 | ⋯ | 0 |
| $\chi_2(2^3P_2)$ | 10.2447 | 10.2245 | 10.261 | 10.271[23], 10.401 [24] | $10.26865 \pm 0.00022 \pm 0.00050$ | 0.7139 | 0.69 | 0 |
| $h_b(3^1P_1)$ | 10.4423 | 10.456 | 10.541 | 10.444 [24] | | 0.9453 | ⋯ | 0 |
| $\chi_0(3^3P_0)$ | 10.4239 | 10.4557 | 10.522 | 10.522 [23], 10.473 [24] | ⋯ | 0.9470 | | 0 |
| $\chi_1(3^3P_1)$ | 10.4396 | 10.4579 | 10.538 | 10.544[23], 10.502 [24] | ⋯ | 0.9476 | | 0 |
| $\chi_2(3^3P_2)$ | 10.4507 | 10.4585 | 10.550 | 10.559[23] | $10.534 \pm 0.009$ | 0.9474 | 0.93 | 0 |
| $h_b(4^1P_1)$ | 10.6213 | 10.6606 | | 10.521 [24] | ⋯ | 1.1541 | ⋯ | 0 |
| $\chi_0(4^3P_0)$ | 10.606 | 10.6607 | 10.775 | 10.550 [24] | ⋯ | 1.1557 | ⋯ | 0 |
| $\chi_1(4^3P_1)$ | 10.619 | 10.6624 | 10.788 | 10.579 [24] | ⋯ | 1.1561 | ⋯ | 0 |
| $\chi_2(4^3P_2)$ | 10.6284 | 10.6627 | 10.798 | ⋯ | ⋯ | 1.1559 | ⋯ | 0 |
| $h_b(5^1P_1)$ | 10.7822 | 10.8459 | 10.790 | ⋯ | ⋯ | 1.3457 | ⋯ | 0 |
| $\chi_0(5^3P_0)$ | 10.7688 | 10.8463 | 11.004 | ⋯ | ⋯ | 1.3472 | ⋯ | 0 |
| $\chi_1(5^3P_1)$ | 10.7802 | 10.8476 | 11.014 | ⋯ | ⋯ | 1.3475 | ⋯ | 0 |

*(Table continued)*

TABLE I. *(Continued)*

| | Our calculated mass | | Theoretical mass | | Experimental mass | Our calculated | Others theor. | Our calculated |
|---|---|---|---|---|---|---|---|---|
| Meson | Relativistic [GeV] | NR [GeV] | Relativistic [20] potential model [GeV] | NR potential model [GeV] | [21] [GeV] | $\sqrt{\langle r^2\rangle}$ [fm] | calculated $\sqrt{\langle r^2\rangle}$ [22] [fm] | $\lvert R(0)\rvert^2$ [GeV$^3$] |
| $\chi_2(5^3P_2)$ | 10.7884 | 10.8478 | 11.022 | ⋯ | ⋯ | 1.3473 | 1.37 | 0 |
| $h_b(6^1P_1)$ | 10.9302 | 11.0176 | 11.016 | ⋯ | ⋯ | 1.5246 | ⋯ | 0 |
| $\chi_0(6^3P_0)$ | 10.9182 | 11.0181 | | ⋯ | ⋯ | 1.5261 | ⋯ | 0 |
| $\chi_1(6^3P_1)$ | 10.9284 | 11.0192 | | ⋯ | ⋯ | 1.5263 | ⋯ | 0 |
| $\chi_2(6^3P_2)$ | 10.9358 | 11.0192 | | ⋯ | ⋯ | 1.5260 | ⋯ | 0 |
| $\eta_{b2}(1^1D_2)$ | 10.1661 | 10.1355 | 10.148 | | ⋯ | 0.5933 | ⋯ | 0 |
| $\Upsilon(1^3D_1)$ | 10.1548 | 10.1299 | 10.138 | | | 0.5930 | ⋯ | 0 |
| $\Upsilon_2(1^3D_2)$ | 10.1649 | 10.1351 | 10.147 | 10.155 [6] | $10.1637 \pm 0.00014$ | 0.5939 | ⋯ | 0 |
| $\Upsilon_3(1^3D_3)$ | 10.1772 | 10.1389 | 10.155 | | ⋯ | 0.5942 | ⋯ | 0 |

| | Our calculated mass | | Relativistic potential | Our calculated | Others theor. |
|---|---|---|---|---|---|
| | Relativistic (GeV) | NR (GeV) | model (GeV) [20] | $\sqrt{\langle r^2\rangle}$ (fm) | calculated $\sqrt{\langle r^2\rangle}$ (fm) [22] |
| Meson | GeV | GeV | GeV | fm | fm |
| $\eta_{b2}(2^1D_2)$ | 10.3801 | 10.3779 | 10.450 | 0.8447 | ⋯ |
| $\Upsilon(2^3D_1)$ | 10.3688 | 10.3751 | 10.441 | 0.8448 | ⋯ |
| $\Upsilon_2(2^3D_2)$ | 10.3789 | 10.378 | 10.449 | 0.8455 | ⋯ |
| $\Upsilon_3(2^3D_3)$ | 10.3864 | 10.3799 | 10.455 | 0.8457 | 0.82 |
| $\eta_{b2}(3^1D_2)$ | 10.5633 | 10.5877 | 10.706 | 1.0634 | ⋯ |
| $\Upsilon(3^3D_1)$ | 10.5525 | 10.5861 | 10.698 | 1.0638 | ⋯ |
| $\Upsilon_2(3^3D_2)$ | 10.5621 | 10.5881 | 10.705 | 1.0643 | ⋯ |
| $\Upsilon_3(3^3D_3)$ | 10.5695 | 10.5892 | 10.711 | 1.0643 | 1.05 |
| $\eta_{b2}(4^1D_2)$ | 10.7273 | 10.777 | 10.935 | 1.2612 | ⋯ |
| $\Upsilon(4^3D_1)$ | 10.717 | 10.776 | 10.928 | 1.2623 | ⋯ |
| $\Upsilon_2(4^3D_2)$ | 10.7262 | 10.7775 | 10.934 | 1.2626 | ⋯ |
| $\Upsilon_3(4^3D_3)$ | 10.7334 | 10.7782 | 10.939 | 1.2625 | 1.27 |
| $\eta_{b2}(5^1D_2)$ | 10.8779 | 10.9518 | | 1.4455 | ⋯ |
| $\Upsilon(5^3D_1)$ | 10.8681 | 10.9512 | | 1.4463 | ⋯ |
| $\Upsilon_2(5^3D_2)$ | 10.8768 | 10.9524 | | 1.4465 | ⋯ |
| $\Upsilon_3(5^3D_3)$ | 10.8839 | 10.9528 | | 14463 | 1.49 |
| $h_{b3}(1^1F_3)$ | 10.3116 | 10.2941 | 10.355 | 0.7280 | ⋯ |
| $\chi_2(1^3F_2)$ | 10.308 | 10.2894 | 10.350 | 0.7266 | ⋯ |
| $\chi_3(1^3F_3)$ | 10.3114 | 10.2937 | 10.355 | 0.728 | ⋯ |
| $\chi_4(1^3F_4)$ | 10.3137 | 10.297 | 10.358 | 0.7289 | ⋯ |
| $h_{b3}(2^1F_3)$ | 10.5 | 10.5102 | 10.619 | 0.9619 | ⋯ |
| $\chi_2(2^3F_2)$ | 10.4956 | 10.5074 | 10.615 | 0.9611 | ⋯ |
| $\chi_3(2^3F_3)$ | 10.4997 | 10.5101 | 10.619 | 0.9619 | ⋯ |
| $\chi_4(2^3F_4)$ | 10.5027 | 10.5119 | 10.622 | 0.9623 | ⋯ |
| $h_{b3}(3^1F_3)$ | 10.6679 | 10.7041 | 10.853 | 1.1688 | ⋯ |
| $\chi_2(3^3F_2)$ | 10.6629 | 10.7022 | 10.850 | 1.1696 | ⋯ |
| $\chi_3(3^3F_3)$ | 10.6676 | 10.7041 | 10.853 | 1.1701 | ⋯ |
| $\chi_4(3^3F_4)$ | 10.6711 | 10.7053 | 10.856 | 1.1702 | ⋯ |
| $h_{b3}(4^1F_3)$ | 10.8216 | 10.8825 | | 1.3621 | ⋯ |
| $\chi_2(4^3F_2)$ | 10.8162 | 10.8811 | | 1.3563 | ⋯ |
| $\chi_3(4^3F_3)$ | 10.8212 | 10.8826 | | 1.3567 | ⋯ |
| $\chi_4(4^3F_4)$ | 10.825 | 10.8835 | | 1.3564 | ⋯ |

of generalized Wilson loops [25]. These energy levels modify the effective $q\bar{q}$ potential $V_{q\bar{q}}(r)$ as

$$V^h_{q\bar{q}}(r) = V_{q\bar{q}}(r) + V_g(r), \tag{6}$$

where $V_g(r)$ represents the contribution of the gluon field to the effective potential. The functional form of $V_g(r)$ depends on the level of gluonic excitation. In this work, we study the hybrid mesons in which the gluonic field is in its first excited state and fit the form of $V_g(r)$,

$$V_g(r) = \frac{c}{r} + A \times \exp^{-\mathrm{Br}^{0.3723}}, \tag{7}$$

for a least difference of resulting gluonic excitation and ground-state energies and the available lattice data [5]. We have shown in Ref. [1] that this proposed form of $V_g(r)$ provides an excellent fit to the lattice data with best-fitted values $A = 3.4693$ GeV, $B = 1.0110$ GeV, and $c = 0.1745$. Thus, for the hybrid mesons, the form of the radial differential equation in Eq. (4) is modified as

$$U''(r) + 2\mu\left(E - V^h_{q\bar{q}}(r) - \frac{\langle L^2_{q\bar{q}}\rangle}{2\mu r^2}\right)U(r) = 0, \tag{8}$$

where the squared quark-antiquark angular momentum $\langle L^2_{q\bar{q}}\rangle$ [5,26] in the leading Born-Oppenheimer approximation is given by

$$\langle L^2_{q\bar{q}}\rangle = L(L+1) - 2\Lambda^2 + \langle J^2_g\rangle. \tag{9}$$

For the first gluonic excitation, the squared gluon angular momentum $\langle J^2_g\rangle = 2$ and $\Lambda$, which is a projection of gluon angular momentum $J_g$ on the $q\bar{q}$ axis, is equal to 1 [5], making $-2\Lambda^2 + \langle J^2_g\rangle = 0$. In Eq. (9), it is assumed that $\mathbf{L} = \mathbf{L}_{q\bar{q}} + \mathbf{J}_g$, which combines with total spin $\mathbf{S}$ of the quark and antiquark to give total angular momentum $\mathbf{J} = \mathbf{L} + \mathbf{S}$ of a hybrid meson.

Using the hybrid potential of Eq. (6), we calculated the masses and radial wave functions of the hybrid mesons by using the same technique as employed for conventional mesons (mentioned above). The effect of the relativistic correction was again determined using the leading-order perturbation theory. The resultant wave functions are plotted in green in Fig. 1, corresponding to the same values of $n$, $L$, and $S$ as used for conventional mesons. The shape of these radial wave functions is changed by the addition of the $V_g$ term for hybrids, and the values of masses are significantly increased for the same values of $n$, $L$, and $S$. These normalized wave functions of conventional and hybrid bottomonium mesons were then used to calculate root-mean-square radii and radial wave functions at origin. The applications of radial wave functions at origin are mentioned above in Sec. I. The leptonic decay widths $\Gamma_{ee}$ of bottomonium mesons for $nS$ states were calculated by the following formula [27]:

$$\Gamma_{ee}(nS) = \frac{4\alpha^2 e_b^2}{M_n^2 s}|R_{nS}(0)|^2\left(1 - \frac{16}{3}\frac{\alpha_s}{\pi} + \Delta(nS)\right). \tag{10}$$

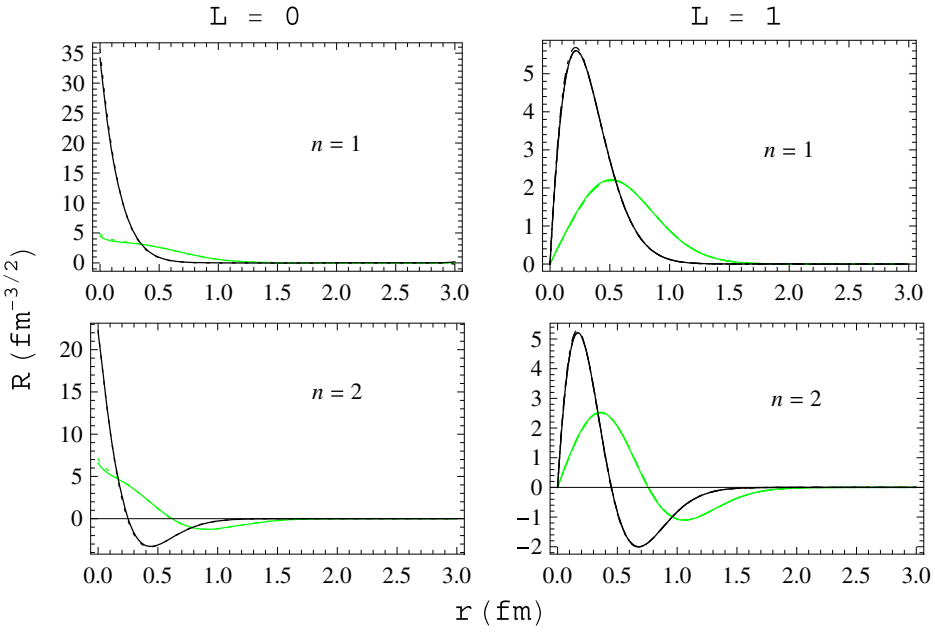


FIG. 1. Radial wave functions for ground and excited states. Black represents conventional, and green color represents hybrid bottomonium mesons. For $L = 0$, wave functions of $\Upsilon$ and $\eta_b$ are almost same. Similarly, for $L = 1$, wave functions of $\chi_{b_0}, \chi_{b_1}, \chi_{b_2}$, and $h_b$ are almost the same within our numerical limits, and so on.

Here, $e_b = -1/3$ is the bottom quark electric charge, and $\alpha$ is the electromagnetic fine structure constant. The second term in parentheses is the leading-order radiative correction, and $\Delta(nS)$ stands for the higher-order radiative and relativistic corrections. The value of $\Delta(nS)$ is state dependent. Following Ref. [27], we fixed it using the experimental value of $\Gamma_{ee}$ for $\Upsilon(4S)$, which is the highest well-known excited S state. We found that for this state $\Delta(nS) = 0.20$. However, the contribution of $\Delta(nS)$ is expected to be small for higher excited states, as in this case relativistic effects are negligible [27]. So, we take it as zero for the excited states higher than $\Upsilon(4S)$. For the $D$ states, leptonic decay widths were calculated by the formula [22]

$$\Gamma_{ee}(nD) = \frac{25\alpha^2 e_b^2}{2M_n^2 D M_b^4}|R''_D(0)|^2\left(1 - \frac{16}{3}\frac{\alpha_s}{\pi}\right). \quad (11)$$

We calculated the two-photon decay transitions for $S$ and $P$ states by using following expressions [22]:

$$\Gamma(^1S_0 \to \gamma\gamma) = \frac{3\alpha^2 e_b^4 |R_{nS}(0)|^2}{m_b^2}, \quad (12)$$

$$\Gamma(^3P_0 \to \gamma\gamma) = \frac{27\alpha^2 e_b^4 |R'_{nP}(0)|^2}{m_b^4}, \quad (13)$$

$$\Gamma(^3P_2 \to \gamma\gamma) = \frac{36\alpha^2 e_b^4 |R'_{nP}(0)|^2}{5m_b^4}. \quad (14)$$

Radiative transitions involve the emission of photon and are important for the study of mesons because they provide a way to access $b\bar{b}$ states with different internal quantum numbers $n$, $L$, $S$, $J$. In $E1$ transitions, orbital quantum numbers are changed, but spin remains same. We calculated the $E1$ radiative partial widths from meson-to-meson transitions by using the following expression mentioned in Ref. [20]:

$$\Gamma_{E1}(n^{2S+1}L_J \to n'^{2S+1}L'_{J'} + \gamma) = \frac{4\alpha e_b^2 k_\gamma^3}{3} C_{fi}\delta_{L,L'\pm1}|\langle\Psi_f|r|\Psi_i\rangle|^2. \quad (15)$$

Here, $k_\gamma$, $E_f^{b\bar{b}}$, and $M_i$ stand for the final photon energy ($E_\gamma = \frac{M_i^2 - M_f^2}{2M_i}$), the energy of the final $b\bar{b}$ meson, and the mass of the initial state of the bottomonium, respectively, and

$$C_{fi} = \max(L, L')(2J' + 1)\begin{Bmatrix} J & 1 & J' \\ L' & S & L \end{Bmatrix}. \quad (16)$$

To calculate the $M1$ radiative partial widths for meson-to-meson transitions, the following expression [20] was used:

$$\Gamma_{M1}(n^{2S+1}L_J \to n'^{2S'+1}L_{J'} + \gamma) = \frac{4\alpha e_b^2 k_\gamma^3}{3m_b^2}\frac{2J' + 1}{2L + 1}\delta_{S,S'\pm1}|\langle\Psi_f|j_0(kr/2)|\Psi_i\rangle|^2. \quad (17)$$

$j_0(x)$ is the spherical Bessel function. We used Eqs. (15) and (17) to calculate both types of radiative transitions, i.e., conventional to conventional and hybrid to hybrid. However, $E1$ transition, which involves the change in $L$, requires some deliberation, as $\mathbf{L}$ includes the contribution of gluon angular momentum $\mathbf{J}_g$. It is noted that the hybrids involved in $E1$ transition are calculated using the gluon potential belonging to the first excitation of gluon field for which $\langle L^2_{q\bar{q}}\rangle = L(L+1)$ by Eq. (9), meaning that the change in $L$ is caused by the corresponding change in $\langle L^2_{q\bar{q}}\rangle$. This gives, according to Eq. (8), the spatial factors of wave functions of initial and final hybrid mesons appearing in Eq. (15). We do not need to change Eq. (15) because hybrid-to-hybrid transitions are between the same gluonic state, as are the conventional-to-conventional transitions; a flux tube model-based analysis [28] of the $E1$ transitions involving hybrids replaces the quarks positions in the $E1$ transition operator by a separable combination of the relative position and a raising operator for the gluonic excitation. This raising operator gives a vanishing contribution to the transition amplitude between the hybrids belonging to same gluonic states, and only the old quarks relative position operator, producing transitions between conventional mesons, produces the $E1$ transitions between hybrid mesons.

## III. RESULTS AND DISCUSSION

The masses, root-mean-square radii, radial wave functions at the origin, leptonic and two-photon decay widths, and radiative transitions are calculated for conventional and hybrid bottomonium mesons including the orbital and radial excited $J^{PC}$ states. The calculated masses of bottomonium mesons using the nonrelativistic and relativistic Hamiltonian for the ground and excited states are given in Table I along with the experimental and theoretical predictions of the other's groups. Table I shows that the lowest bottomonium meson's mass is ≈9.5 GeV. Masses for hybrid bottomonium mesons using the nonrelativistic and relativistic Hamiltonian for the ground state, orbital, and radial excited states are reported in Table II. For differentiating the symbols of conventional and hybrid mesons, a superscript $h$ is used with the corresponding conventional meson symbol having the same values of $n$, $L$, and $S$. This is the same convention used earlier in our Ref. [3]. In our calculations, the lowest hybrid bottomonium has $J^{PC} = 0^{++}(0^{--})$ with mass equal to 10.8069 GeV that is comparable to results mentioned in

TABLE II. Our calculated masses; root-mean-square radii; and radial wave function at the origin for ground, radial, and orbital excited states $b\bar{b}$ hybrid bottomonium mesons.

| | $J^{PC}$ | | Our calculated mass | | Our calculated calculated $\sqrt{\langle r^2 \rangle}$ | Our calculated $\lvert R(0)\rvert^2$ |
|---|---|---|---|---|---|---|
| Meson | $\varepsilon = 1$ | $\varepsilon = -1$ | Relativistic [GeV] | NR [GeV] | [fm] | [GeV$^3$] |
| $\eta_b^h(1^1S_0)$ | $0^{++}$ | $0^{--}$ | 10.8069 | 10.7734 | 0.6215 | 0.1445 |
| $\Upsilon^h(1^3S_1)$ | $1^{+-}$ | $1^{-+}$ | 10.8079 | 10.7747 | 0.6272 | 0.1281 |
| $\eta_b^h(2^1S_0)$ | $0^{++}$ | $0^{--}$ | 10.9262 | 10.9187 | 0.874 | 0.3448 |
| $\Upsilon^h(2^3S_1)$ | $1^{+-}$ | $1^{-+}$ | 10.928 | 10.9211 | 0.8801 | 0.3115 |
| $\eta_b^h(3^1S_0)$ | $0^{++}$ | $0^{--}$ | 11.0459 | 11.0636 | 1.0977 | 0.4873 |
| $\Upsilon^h(3^3S_1)$ | $1^{+-}$ | $1^{-+}$ | 11.048 | 11.0664 | 1.1027 | 0.4520 |
| $\eta_b^h(4^1S_0)$ | $0^{++}$ | $0^{--}$ | 11.1642 | 11.2057 | 1.3000 | 0.5727 |
| $\Upsilon^h(4^3S_1)$ | $1^{+-}$ | $1^{-+}$ | 11.1662 | 11.2086 | 1.3039 | 0.5425 |
| $\eta_b^h(5^1S_0)$ | $0^{++}$ | $0^{--}$ | 11.2798 | 11.3442 | 1.4864 | 0.6245 |
| $\Upsilon^h(5^3S_1)$ | $1^{+-}$ | $1^{-+}$ | 11.2817 | 11.3469 | 1.4895 | 0.6003 |
| $\eta_b^h(6^1S_0)$ | $0^{++}$ | $0^{--}$ | 11.3924 | 11.4789 | 1.6606 | 0.6579 |
| $\Upsilon^h(6^3S_1)$ | $1^{+-}$ | $1^{-+}$ | 11.394 | 11.4814 | 1.6632 | 0.6385 |
| $h_b^h(1^1P_1)$ | $1^{--}$ | $1^{++}$ | 10.8561 | 10.8357 | 0.7601 | 0 |
| $\chi_0^h(1^3P_0)$ | $0^{-+}$ | $0^{+-}$ | 10.8534 | 10.8325 | 0.7564 | 0 |
| $\chi_1^h(1^3P_1)$ | $1^{-+}$ | $1^{+-}$ | 10.8559 | 10.8354 | 0.7594 | 0 |
| $\chi_2^h(1^3P_2)$ | $2^{-+}$ | $2^{+-}$ | 10.8569 | 10.8366 | 0.7623 | 0 |
| $h_b^h(2^1P_1)$ | $1^{--}$ | $1^{++}$ | 10.984 | 10.9889 | 1.0014 | 0 |
| $\chi_0^h(2^3P_0)$ | $0^{-+}$ | $0^{+-}$ | 10.9792 | 10.9868 | 0.9996 | 0 |
| $\chi_1^h(2^3P_1)$ | $1^{-+}$ | $1^{+-}$ | 10.9835 | 10.989 | 1.0015 | 0 |
| $\chi_2^h(2^3P_2)$ | $2^{-+}$ | $2^{+-}$ | 10.9856 | 10.9897 | 1.0035 | 0 |
| $h_b^h(3^1P_1)$ | $1^{--}$ | $1^{++}$ | 11.1074 | 11.1363 | 1.2126 | 0 |
| $\chi_0^h(3^3P_0)$ | $0^{-+}$ | $0^{+-}$ | 11.1012 | 11.135 | 1.2115 | 0 |
| $\chi_1^h(3^3P_1)$ | $1^{-+}$ | $1^{+-}$ | 11.1066 | 11.1367 | 1.2131 | 0 |
| $\chi_2^h(3^3P_2)$ | $2^{-+}$ | $2^{+-}$ | 11.1097 | 11.1372 | 1.2149 | 0 |
| $h_b^h(4^1P_1)$ | $1^{--}$ | $1^{++}$ | 11.2266 | 11.2786 | 1.4048 | 0 |
| $\chi_0^h(4^3P_0)$ | $0^{-+}$ | $0^{+-}$ | 11.2195 | 11.2777 | 1.4041 | 0 |
| $\chi_1^h(4^3P_1)$ | $1^{-+}$ | $1^{+-}$ | 11.2257 | 11.2791 | 0.7564 | 0 |
| $\chi_2^h(4^3P_2)$ | $2^{-+}$ | $2^{+-}$ | 11.2293 | 11.2795 | 1.4071 | 0 |
| $h_b^h(5^1P_1)$ | $1^{1--}$ | $1^{++}$ | 11.3418 | 11.4161 | 1.5834 | 0 |
| $\chi_0^h(5^3P_0)$ | $0^{-+}$ | $0^{+-}$ | 11.3342 | 11.4155 | 1.5829 | 0 |
| $\chi_1^h(5^3P_1)$ | $1^{-+}$ | $1^{+-}$ | 11.3408 | 11.4167 | 1.5841 | 0 |
| $\chi_2^h(5^3P_2)$ | $2^{-+}$ | $2^{+-}$ | 11.3448 | 11.417 | 1.5858 | 0 |
| $h_b^h(6^1P_1)$ | $1^{--}$ | $1^{++}$ | 11.4534 | 11.5493 | 1.7514 | 0 |
| $\chi_0^h(6^3P_0)$ | $0^{-+}$ | $0^{+-}$ | 11.4456 | 11.549 | 1.7512 | 0 |
| $\chi_1^h(6^3P_1)$ | $1^{-+}$ | $1^{+-}$ | 11.4524 | 11.5501 | 1.7521 | 0 |
| $\chi_2^h(6^3P_2)$ | $2^{-+}$ | $2^{+-}$ | 11.4566 | 11.5503 | 1.7538 | 0 |
| $\eta_{b2}(1^1D_2)$ | $2^{++}$ | $2^{--}$ | 10.9125 | 10.9053 | 0.8771 | 0 |
| $\Upsilon^h(1^3D_1)$ | $1^{+-}$ | $1^{-+}$ | 10.9119 | 10.9032 | 0.8726 | 0 |
| $\Upsilon_2^h(1^3D_2)$ | $2^{+-}$ | $2^{-+}$ | 10.9126 | 10.9052 | 0.8761 | 0 |
| $\Upsilon_3^h(1^3D_3)$ | $3^{+-}$ | $3^{-+}$ | 10.9127 | 10.9063 | 0.8799 | 0 |
| $\eta_{b2}^h(2^1D_2)$ | $2^{++}$ | $2^{--}$ | 11.0409 | 11.0583 | 1.1058 | 0 |
| $\Upsilon^h(2^3D_1)$ | $1^{+-}$ | $1^{-+}$ | 11.0395 | 11.0566 | 1.1025 | 0 |

*(Table continued)*

TABLE II. *(Continued)*

| | $J^{PC}$ | | Our calculated mass | | Our calculated calculated $\sqrt{\langle r^2\rangle}$ | Our calculated $\lvert R(0)\rvert^2$ |
|---|---|---|---|---|---|---|
| Meson | $\varepsilon=1$ | $\varepsilon=-1$ | Relativistic [GeV] | NR [GeV] | [fm] | [GeV$^3$] |
| $\Upsilon_2^h(2^3D_2)$ | $2^{+-}$ | $2^{-+}$ | 11.0408 | 11.0582 | 1.1051 | 0 |
| $\Upsilon_3^h(2^3D_3)$ | $3^{+-}$ | $3^{-+}$ | 11.0415 | 11.0591 | 1.1080 | 0 |

| | $J^{PC}$ | | Our calculated mass | | |
|---|---|---|---|---|---|
| Meson | $\varepsilon=1$ | $\varepsilon=-1$ | Relativistic [GeV] | NR [GeV] | Calculated $\sqrt{\langle r^2\rangle}$ [fm] |
| $\eta_{b2}^h(3^1D_2)$ | $2^{++}$ | $2^{--}$ | 11.1639 | 11.2047 | 1.3087 |
| $\Upsilon^h(3^3D_1)$ | $1^{+-}$ | $1^{-+}$ | 11.1618 | 11.2034 | 1.3059 |
| $\Upsilon_2^h(3^3D_2)$ | $2^{+-}$ | $2^{-+}$ | 11.1638 | 11.2048 | 1.3081 |
| $\Upsilon_3^h(3^3D_3)$ | $3^{+-}$ | $3^{-+}$ | 11.165 | 11.2054 | 1.3108 |
| $\eta_{b2}^h(4^1D_2)$ | $2^{++}$ | $2^{--}$ | 11.2823 | 11.3457 | 1.4947 |
| $\Upsilon^h(4^3D_1)$ | $1^{+-}$ | $1^{-+}$ | 11.2796 | 11.3446 | 1.4922 |
| $\Upsilon_2^h(4^3D_2)$ | $2^{+-}$ | $2^{-+}$ | 11.2821 | 11.3458 | 1.4943 |
| $\Upsilon_3^h(4^3D_3)$ | $3^{+-}$ | $3^{-+}$ | 11.2837 | 11.3463 | 1.4969 |
| $\eta_{b2}^h(1^1D_2)$ | $2^{++}$ | $2^{--}$ | 11.3965 | 11.4818 | 1.6685 |
| $\Upsilon^h(5^3D_1)$ | $1^{+-}$ | $1^{-+}$ | 11.3933 | 11.4809 | 1.6661 |
| $\Upsilon_2^h(5^3D_2)$ | $2^{+-}$ | $2^{-+}$ | 11.3962 | 11.4819 | 1.6682 |
| $\Upsilon_3^h(5^3D_3)$ | $3^{+-}$ | $3^{-+}$ | 11.3983 | 11.4823 | 1.6707 |
| $h_{b3}^h(1^1F_3)$ | $3^{--}$ | $3^{++}$ | 10.9727 | 10.9787 | 0.9856 |
| $\chi_2^h(1^3F_2)$ | $2^{-+}$ | $2^{+-}$ | 10.9729 | 10.9774 | 0.9806 |
| $\chi_3^h(1^3F_3)$ | $3^{-+}$ | $3^{+-}$ | 10.9729 | 10.9787 | 0.9847 |
| $\chi_4^h(1^3F_4)$ | $4^{-+}$ | $4^{+-}$ | 10.9724 | 10.9793 | 0.9891 |
| $h_{b3}^h(2^1F_3)$ | $3^{--}$ | $3^{++}$ | 11.0995 | 11.1293 | 1.2029 |
| $\chi_2^h(2^3F_2)$ | $2^{-+}$ | $2^{+-}$ | 11.0993 | 11.1281 | 1.1989 |
| $\chi_3^h(2^3F_3)$ | $3^{-+}$ | $3^{+-}$ | 11.0996 | 11.1293 | 1.2023 |
| $\chi_4^h(2^3F_4)$ | $4^{-+}$ | $4^{+-}$ | 11.0995 | 11.13 | 1.206 |
| $h_{b3}^h(3^1F_3)$ | $3^{--}$ | $3^{++}$ | 11.221 | 11.2736 | 1.3983 |
| $\chi_2^h(3^3F_2)$ | $2^{-+}$ | $2^{+-}$ | 11.2204 | 11.2725 | 1.3947 |
| $\chi_3^h(3^3F_3)$ | $3^{-+}$ | $3^{+-}$ | 11.221 | 11.2737 | 1.3977 |
| $\chi_4^h(3^3F_4)$ | $4^{-+}$ | $4^{+-}$ | 11.2212 | 11.2742 | 1.4012 |
| $h_{b3}^h(4^1F_3)$ | $3^{--}$ | $3^{++}$ | 11.3378 | 11.4126 | 1.5777 |
| $\chi_2^h(4^3F_2)$ | $2^{-+}$ | $2^{+-}$ | 11.3369 | 11.4116 | 1.5759 |
| $\chi_3^h(4^3F_3)$ | $3^{-+}$ | $3^{+-}$ | 11.3378 | 11.4126 | 1.5785 |
| $\chi_4^h(4^3F_4)$ | $4^{-+}$ | $4^{+-}$ | 11.3383 | 11.4131 | 1.5817 |

Ref. [8]. A comparison of Tables I and II shows that how much the mass of a hybrid meson is more than that of the corresponding conventional meson with same quantum numbers ($n$, $L$, and $S$). It is noted that $J^{PC}$ of each hybrid meson is different from the corresponding conventional meson for the same $L$ and $S$. This difference is due to additional quantum numbers ($\Lambda$, $\varepsilon$, and $\eta$) present in the squared quark-antiquark angular momentum term for hybrid mesons defined in Eq. (9) and in the following expressions for the parity $P$ and charge parity $C$ of hybrid mesons,

$$P=\varepsilon(-1)^{L+\Lambda+1}, \qquad C=\varepsilon\eta(-1)^{L+\Lambda+S}, \tag{18}$$

where $\Lambda=0,1,2,\ldots$ correspond to the states represented by symbols $\Sigma,\Pi_u,\Delta,\ldots$ in Ref. [5]. Here, $\Sigma$ represents the mesons with the ground-state gluonic field, $\Pi_u$ corresponds to the mesons with the first excited-state gluonic field, and

TABLE III. Masses (in GeV) of hybrid bottomonium mesons calculated by other models along with our calculated results. Our results are reported for $J^{PC}$ states with lowest orbital angular momentum (L).

| | Our results | | Non-relativistic lattice QCD (NRLQCD) | | | | | |
|---|---|---|---|---|---|---|---|---|
| $J^{PC}$ Sate | Ground state | First radial excited state | Ground state [6] | First radial [6] | Lattice QCD (LQCD) [6] | QCD sum rule [17,30] | Constituent gluon model [7] | Quark model and Quark Confining String (QCS) [31] |
| $0^{--}$ | 10.8069 | 10.9262 | ⋯ | | ⋯ | $11.48 \pm 0.75$ | 10.66 | |
| $1^{--}$ | 10.8561 | 10.984 | 10.559 | $10.977 + 0.041$ | | $9.7 \pm 0.12$ | 10.50 | 10.785 |
| $0^{-+}$ | 10.8534 | 10.9792 | | | | $9.68 \pm 0.29$ | 10.68 | |
| $1^{-+}$ | 10.8079 | 10.928 | | | 10.559 | $9.79 \pm 0.22$ | 10.80 | |
| $1^{+-}$ | 10.8079 | 10.928 | | | | $10.70 \pm 0.53$ | | |
| $0^{+-}$ | 10.8534 | 10.9792 | | ⋯ | $10.159 \pm 0.362$ | $10.17 \pm 0.22$ | | |
| $1^{++}$ | 10.8561 | 10.984 | $10.597 \pm 0.065$ | ⋯ | ⋯ | $11.09 \pm 0.60$ | ⋯ | |
| $0^{++}$ | 10.8069 | 10.9262 | $10.892 \pm 0.036$ | ⋯ | ⋯ | $11.20 \pm 0.48$ | ⋯ | |
| $2^{+-}$ | 10.8569 | 10.9856 | ⋯ | ⋯ | $11.323 \pm 0.257$ | ⋯ | ⋯ | |
| $2^{-+}$ | 10.8569 | 10.9856 | ⋯ | ⋯ | | $9.93 \pm 0.21$ | ⋯ | |
| $2^{++}$ | 10.9125 | 11.0409 | ⋯ | ⋯ | | $10.64 \pm 0.33$ | ⋯ | |

so on. $\eta = -1$, and $\varepsilon = \pm 1$ for the $\Pi_u$ state [5]. It is noted that parameter $\varepsilon$ has two possible values $+1$ and $-1$ for the first gluonic excited state, which we include in the study of hybrid mesons in our present work. As a result, we obtain two degenerate hybrid states with opposite values of $P$ and $C$. (This degeneracy has been recently discussed in Ref. [29] along with the nature of the approximation of using this in QCD.) For $\varepsilon = 1$, the hybrid mesons are nonexotic, whereas exotic hybrid mesons are obtained for $\varepsilon = -1$ as shown in the Table II.

The comparison of our calculated masses of bottomonium hybrid mesons with those by others is given in Table III. We do not get as large differences in bottomonium hybrid masses predictions as lattice QCD-based and sum rules-based works report. But the constituent gluon model approach of Ref. [7] has differences comparable to ours. For $J^{PC} = 1^{-+}$, we almost have agreement with Ref. [7]. Our calculations give 10.8069 GeV for the mass of the lightest hybrid in the bottomonium sector without any radial excitation. This has $J^{PC} = 0^{--}$. Reference [7] reports the lightest hybrid meson to have a mass of 10.50 GeV with $J^{PC} = 1^{--}$. The calculations reported in Refs. [17] and [30] using the QCD sum rule give the lightest hybrid mass as low as 9.68 GeV with $J^{PC} = 0^{-+}$. This is part of their lightest hybrid supermultiplet. They take corresponding positive parity states belonging to the heavier hybrid supermultiplet starting from 10.17 GeV. But in the leading BO approximation, the $\Pi_u^+$ potential is the same as that for $\Pi_u^-$ [5,6], meaning that both parity states have the same mass. We use leading-order BO approximation and thus have the same mass for both parities and both hybrid supermultiplets. Reference [6] arbitrarily chose the mass of the $1^{--}$ member of their ground-state $H_1$ multiplet, as defined in their Ref. [46], to be the $B\bar{B}$ threshold, i.e., 10.559 GeV, and used the splittings from their Ref. [14] to estimate the masses of the other bottomonium hybrids in lattice non-relativistic QCD (NRQCD). These masses remained heavier than the chosen $1^{--}$ mass of 10.559 GeV. When they repeated the same procedure for the lattice QCD, this time choosing the $1^{-+}$ member of the ground-state $H_1$ multiplet, they got the light bottomonium hybrid to be 10.159 GeV with $J^{PC} = 0^{+-}$ having significant statistical errors of the lattice calculations and uncertainties from setting the heavy-quark mass. Reference [6] reports 440 MeV difference between the masses of the $1^{--}$ states in their radially ground and excited multiplets, which is significantly more than our corresponding difference of 128 MeV. The quark confining string model has been used [31] recently in QCD multipole expansion. For the radially ground state (i.e., $n = 1$), the only value they needed and calculated, their calculated mass was 10.785 GeV with $J^{PC} = 1^{--}$, which is not much different than our corresponding hybrid mass. A closely related vibrating string (flux tube) model used in Ref. [32] has nearly the same value, i.e., 10.789 GeV, resulting from their model 3, but their model 1 gives a hybrid meson mass as 10.560 GeV.

Our root-mean-square radii and radial wave functions at the origin for the ground and orbitally and radially excited

TABLE IV. Our calculated leptonic decay widths.

| State | Conventional (keV) | Experimental | Hybrid (keV) |
|---|---|---|---|
| $1^3S_1$ | 1.574 | $1.34 \pm 0.018$ | 0.0135 |
| $2^3S_1$ | 0.496 | $0.612 \pm 0.011$ | 0.0322 |
| $3^3S_1$ | 0.337 | $0.443 \pm 0.008$ | 0.0457 |
| $4^3S_1$ | 0.272 | $0.272 \pm 0.029$ | 0.0537 |
| $5^3S_1$ | 0.230 | $0.31 \pm 0.07$ | 0.0582 |
| $6^3S_1$ | 0.209 | $0.13 \pm 0.030$ | 0.0607 |
| $1^3D_1$ | 0.241 | ⋯ | 0.0016 |
| $2^3D_1$ | 0.314 | ⋯ | 0.0033 |
| $3^3D_1$ | 0.195 | ⋯ | 0.0294 |

TABLE V. Our calculated two-photon decay widths.

| State | Conventional (keV) | Hybrid (keV) |
|---|---|---|
| $1^1S_0$ | 0.813 | 0.0119 |
| $2^1S_0$ | 0.271 | 0.0257 |
| $3^1S_0$ | 0.195 | 0.0348 |
| $4^1S_0$ | 0.165 | 0.0403 |
| $5^1S_0$ | 0.148 | 0.0438 |
| $6^1S_0$ | 0.136 | 0.0461 |
| $1^3P_0$ | 0.354 | 0.00497 |
| $2^3P_0$ | 0.346 | 0.00216 |
| $3^3P_0$ | 0.284 | 0.00530 |
| $1^3P_2$ | 0.109 | 0.000548 |
| $2^3P_2$ | 0.105 | 0.003512 |
| $3^3P_2$ | 0.139 | 0.00971 |

states of conventional and hybrid bottomonium mesons are also reported in Tables I and II, respectively. We used the wave function at the origin to calculate leptonic and two-photon decay widths of conventional and hybrid bottomonium mesons using Eqs. (10) to (14). Our calculated widths are given in Tables IV and V, along with the corresponding available experimental data. The annihilation of the quarks takes place at the scale defined by the Compton wavelength $1/m_q$, which is close to zero for heavy quarks, and hence the decay constant of a quarkonium state is proportional to the square of its wave function at the origin. Our results of wave functions at the origin for conventional bottomonia given in Table I show that their values decrease with $n$, which implies that decay rates also decrease with an increase in $n$ as shown in Table IV. This result is consistent with the experimental values of the decay rates given in the table. However, in the case of hybrid mesons, the wave function at the origin increases with $n$ as shown in Table II. It is also noted that the wave function at the origin for a hybrid state is significantly lower than for the same conventional states. This makes decay widths of hybrids much lower than the conventional bottomonium mesons as shown in Tables IV and V. Thus, the hybrid states are characteristically different from

TABLE VI. $S \to P$, $E1$ radiative transitions. Experimental results with a † sign are calculated by considering the experimental measured branching ratio [37] and total decay width calculated in Ref. [20]. We use the experimental masses if known. Where experimental masses are not available theoretically calculated masses are used given in Tables I and II.

| Transition | Initial meson | Final meson | Our calculated $\Gamma_{E1}$ NR [keV] | Our calculated $\Gamma_{E1}$ Relativistic [keV] | Exp. [37] calculated $\Gamma_{E1}$ keV | Others theor. [20] calculated $\Gamma_{E1}$ keV | Our calculated $\Gamma_{E1}$ for hybrid NR [keV] | Our calculated $\Gamma_{E1}$ for hybrid Relativistic [keV] |
|---|---|---|---|---|---|---|---|---|
| $2S \to 1P$ | $\Upsilon(2^3S_1)$ | $\chi_2(1^3P_2)$ | 2.92446 | 3.1721 | $2.29 \pm 0.23$ | 1.88 | 1.7016 | 1.1754 |
| | | $\chi_1(1^3P_1)$ | 2.8324 | 3.0722 | $2.21 \pm 0.22$ | 1.63 | 1.0648 | 0.7353 |
| | | $\chi_0(1^3P_0)$ | 1.8530 | 2.0099 | $1.22 \pm 0.16$ | 0.91 | 0.3919 | 0.2713 |
| | $\eta_b(2^1S_0)$ | $h_b(1^1P_1)$ | 4.5379 | 6.1059 | | 2.48 | 2.9962 | 2.0837 |
| $3S \to 2P$ | $\Upsilon(3^3S_1)$ | $\chi_2(2^3P_2)$ | 3.5085 | 3.9429 | $2.66 \pm 0.41$ | 2.3 | 2.8476 | 1.8071 |
| | | $\chi_1(2^3P_1)$ | 3.2114 | 3.60897 | $2.56 \pm 0.34$ | 1.91 | 1.7555 | 1.9948 |
| | | $\chi_0(2^3P_0)$ | 1.9819 | 2.2273 | $1.2 \pm 0.16$ | 1.03 | 0.6362 | 0.4837 |
| | $\eta_b(3^1S_0)$ | $h_b(2^1P_1)$ | 3.3529 | 1.0037 | ⋯ | | 4.9051 | 3.2650 |
| $3S \to 1P$ | $\Upsilon(3^3S_1)$ | $\chi_2(1^3P_2)$ | 0.478 | 0.8894 | $0.20 \pm 0.03$ | 0.45 | 0.00082 | 0.0001752 |
| | | $\chi_1(1^3P_1)$ | 0.3247 | 0.6041 | $0.018 \pm 0.010$ | 0.05 | 0.00050 | 0.0001779 |
| | | $\chi_0(1^3P_0)$ | 0.1323 | 0.2461 | $0.055 \pm 0.010$ | 0.01 | 0.00017 | 0.00003697 |
| | $\eta_b(3^1S_0)$ | $h_b(1^1P_1)$ | 0.7162 | 1.0104 | ⋯ | | 0.00075 | 0.003845 |
| $4S \to 3P$ | $\Upsilon(4^3S_1)$ | $\chi_2(3^3P_2)$ | 16.1868 | 22.1972 | | 0.82 | 3.7232 | 2.1898 |
| | | $\chi_1(3^3P_1)$ | 9.8560 | 17.0252 | | 0.84 | 2.2809 | 1.5411 |
| | | $\chi_0(3^3P_0)$ | 3.4652 | 7.7808 | | 0.48 | 0.8152 | 0.6656 |
| | $\eta_b(4^1S_0)$ | $h_b(3^1P_1)$ | 4.6883 | 1.5278 | | 1.24 | 6.3651 | 4.1018 |
| $4S \to 2P$ | $\Upsilon(4^3S_1)$ | $\chi_2(2^3P_2)$ | 0.2995 | 0.5918 | ⋯ | | 0.00052 | 0.002269 |
| | | $\chi_1(2^3P_1)$ | 0.2029 | 0.401 | ⋯ | | 0.00031 | 0.002348 |
| | | $\chi_0(2^3P_0)$ | 0.0826 | 0.1632 | ⋯ | | 0.00011 | 0.000503 |
| | $\eta_b(4^1S_0)$ | $h_b(2^1P_1)$ | 0.5538 | 0.5644 | | | 0.0041 | 0.0150 |
| $4S \to 1P$ | $\Upsilon(4^3S_1)$ | $\chi_2(^3P_2)$ | 0.2212 | 0.3857 | ⋯ | | 0.0033 | 0.006019 |
| | | $\chi_1(^3P_1)$ | 0.144 | 0.251 | ⋯ | | 0.0021 | 0.006076 |
| | | $\chi_0(^3P_0)$ | 0.0549 | 0.0957 | ⋯ | | 0.00069 | 0.001244 |
| | $\eta_b(4^1S_0)$ | $h_b(^1P_1)$ | 0.361 | 0.4644 | ⋯ | | 0.0146 | 0.01693 |

conventional states as their leptonic and two-photon decay rates are smaller and also increasing functions of $n$ as shown in Tables IV and V. This result can be very useful in finding the clues of hybrids in the experimental data. Our results in Tables I and II also show that for the same quantum numbers ($n$, $L$, and $S$) root-mean-square radii of hybrid mesons are greater than conventional mesons. It is also noted that radii of conventional and hybrid mesons increase with radial and angular excitations.

Our calculated radiative magnetic dipole ($M1$) transitions and electric dipole ($E1$) transitions are reported in Tables VI–XI using the relativistic and nonrelativistic masses. In the $M1$ transitions, the initial and final states belong to the same orbital excitation but have different spins, and in the $E1$ transitions, the orbital quantum numbers of initial and final states are changed, but spins remain the same. Radiative transitions of excited bottomonium states are important because they provide a way to access $b\bar{b}$ states with different internal quantum numbers $(n, L, S, J)$. $\chi_b(1P)$ and $\chi_b(2P)$ states have been studied experimentally through the radiative decays of $\Upsilon(2S)$ and $\Upsilon(3S)$ states [33]. Recently, the ATLAS Collaboration and LHCb reconstructed the $\chi_b(1P, 2P, 3P)$ states through the radiative decay $\chi_b(nP) \to \Upsilon(1S, 2S)$ [34]. It is noted that $E1$ radiative transitions are typically of order of 1 to 10 keV, whereas $M1$ transitions are reduced due to the $m_b^2$ factor in the formula. Nevertheless, $M1$ transitions have been useful in observing spin singlet states that are difficult to observe otherwise. It is also found that $E1$ transitions are suppressed for transition between the states that differ by two radial nodes like $5S \to 3P$, $3P \to 1D$, $4P \to 2S$, $4D \to 2S$, $4D \to 2P$, and $3D \to 1F$ [35] except the $3P \to 1S$. We find same behavior in the case of radiative transitions of hybrid $b\bar{b}$ states. Generally, both $E1$ and $M1$ transition rates are also very small when the transitions occur between the states with close masses because of the reduced value of $E_\gamma$, whereas the transition rates of strong decays are of order of a few MeV [20]. As a result, the branching ratios of radiative transitions are significantly reduced when strong decays open at the threshold of $B\bar{B}$ states of energy 10.56 GeV. Thus, branching ratios of radiative transition can be significantly high for the conventional $1S$, $2S$, $3S$, $1P$, $2P$, $3P$, $1D$, $2D$, $1F$, and $1G$ states having mass less than 10.56 GeV. In the case of hybrids states, the branching ratios of radiative transitions are expected to be small because the mass of even the lightest hybrid states is greater than the $B\bar{B}$ channel threshold, and hence competing strong decays are open for all hybrids. In Tables VI–XI, the comparison of the decay widths of radiative transitions of conventional and hybrid $b\bar{b}$ states with the available experimental data and results of Refs. [20,36] is provided. For most of the transitions, the results are comparable to available experiments and other theoretical models. Reported values of decay widths of radiative transitions

TABLE VII. 1P and 2P, $E1$ radiative transitions.

| Transition | Initial meson | Final meson | Our calculated $\Gamma_{E1}$ | | Exp. $\Gamma_{E1}$ | Others theor. [20] $\Gamma_{E1}$ | Our calculated $\Gamma_{E1}$ for hybrid | |
|---|---|---|---|---|---|---|---|---|
| | | | NR [keV] | Relativistic [keV] | [keV] | [keV] | NR [keV] | relativistic [keV] |
| $1P \to 1S$ | $\chi_2(1^3P_2)$ | $\Upsilon(1^3S_1)$ | 37.2672 | 32.4094 | $34.38^\dagger$ | 32.8 | 0.8501 | 0.5231 |
| | $\chi_1(1^3P_1)$ | | 32.8195 | 14.0823 | $32.544^\dagger$ | 29.5 | 0.8018 | 0.4918 |
| | $\chi_0(1^3P_0)$ | | 26.0114 | 11.1611 | $--^\dagger$ | 23.8 | 0.6928 | 0.4192 |
| | $h_b(1^1P_1)$ | $\eta_b(1^1S_0)$ | 22.8589 | 23.0341 | $35.77^\dagger$ | 35.7 | 0.8515 | 0.5217 |
| $2P \to 2S$ | $\chi_2(2^3P_2)$ | $\acute{\Upsilon}_2(2^3S_1)$ | 18.9917 | 17.9986 | $24.645^\dagger$ | 14.3 | 1.7320 | 1.2147 |
| | $\chi_1(2^3P_1)$ | | 16.1418 | 15.2977 | $23.283^\dagger$ | 13.3 | 1.6798 | 1.0871 |
| | $\chi_0(2^3P_0)$ | | 11.8767 | 11.2557 | $0.0001196^\dagger$ | 10.9 | 1.5225 | 0.8543 |
| | $h_b(2^1P_1)$ | $\acute{\eta}_b(2^1S_0)$ | 12.793 | 13.065 | $40.32^\dagger$ | 14.1 | 1.8030 | 1.1985 |
| $2P \to 1S$ | $\chi_2(2^3P_2)$ | $\Upsilon(1^3S_1)$ | 14.3444 | 16.5078 | $16.275^\dagger$ | 8.4 | 0.0828 | 0.0803 |
| | $\chi_1(2^3P_1)$ | | 13.6951 | 7.7764 | $10.764^\dagger$ | 5.5 | 0.0820 | 0.0775 |
| | $\chi_0(2^3P_0)$ | | 12.6092 | 7.1582 | $0.0000234^\dagger$ | 2.5 | 0.0796 | 0.072 |
| | $h_b(2^1P_1)$ | $\eta_b(1^1S_0)$ | 10.4703 | 12.9422 | $18.48^\dagger$ | 13.0 | 0.0612 | 0.0641 |
| $2P \to 1D$ | $\chi_2(2^3P_2)$ | $\Upsilon_3(1^3D_3)$ | 2.8853 | 2.1582 | | 1.5 | 1.6931 | 1.2894 |
| | | $\Upsilon_2(1^3D_2)$ | 1.0543 | 0.5806 | | 0.3 | 0.3144 | 0.2312 |
| | | $\Upsilon(1^3D_1)$ | 0.07872 | 0.0493 | | 0.03 | 0.0225 | 0.0158 |
| | $\chi_1(2^3P_1)$ | $\Upsilon_2(1^3D_2)$ | 3.8710 | 1.9464 | | 1.2 | 1.5334 | 1.0596 |
| | | $\Upsilon(1^3D_1)$ | 1.4630 | 0.8546 | | 0.5 | 0.5484 | 0.3637 |
| | $\chi_0(2^3P_0)$ | $\Upsilon(1^3D_1)$ | 3.2108 | 1.5811 | | 1.0 | 2.0300 | 1.2093 |
| | $h_b(2^1P_1)$ | $\eta_{2b}(1^1D_2)$ | 1.9096 | 1.0775 | | 1.7 | 2.0379 | 1.4554 |

TABLE VIII. 3P $E1$ radiative transitions.

| Transition | Initial meson | Final meson | Our calculated $\Gamma_{E1}$ NR [keV] | Our calculated $\Gamma_{E1}$ Relativistic [keV] | Others theor. calculated $\Gamma_{E1}$ keV | Our calculated $\Gamma_{E1}$ for hybrid NR [keV] | Our calculated $\Gamma_{E1}$ for hybrid Relativistic [keV] |
|---|---|---|---|---|---|---|---|
| $3P \to 3S$ | $\chi_2(3^3P_2)$ | $\Upsilon(3^3S_1)$ | 2.7868 | 2.1708 | 8.2 [36] | 2.5898 | 1.9761 |
| | $\chi_1(3^3P_1)$ | | 2.7389 | 1.5024 | 7.4 [36] | 2.5356 | 1.6942 |
| | $\chi_0(3^3P_0)$ | | 2.568 | 0.8133 | 6.1 [36] | 2.3569 | 1.2692 |
| | $h_b(3^1P_1)$ | $\eta_b(3^1S_0)$ | 2.53206 | 10.5692 | 8.9 [20] | 2.71248 | 1.9078 |
| $3P \to 2S$ | $\chi_2(3^3P_2)$ | $\acute{\Upsilon}(2^3S_1)$ | 3.8179 | 4.4072 | 3.8 [36] | 0.02522 | 0.02428 |
| | $\chi_1(3^3P_1)$ | | 3.8027 | 4.0832 | 2.5 [36] | 0.02505 | 0.0231 |
| | $\chi_0(3^3P_0)$ | | 3.7472 | 3.6518 | 1.2 [36] | 0.02447 | 0.02107 |
| | $h_b(3^1P_1)$ | $\eta_b(2^1S_0)$ | 4.3418 | 4.45835 | 8.2 [20] | 0.0085 | 0.01186 |
| $3P \to 1S$ | $\chi_2(3^3P_2)$ | $\Upsilon(1^3S_1)$ | 6.5022 | 4.087 | 3.9 [36] | 0.02377 | 0.0182 |
| | $\chi_1(3^3P_1)$ | | 6.4914 | 3.9609 | 2.1 [36] | 0.02367 | 0.01762 |
| | $\chi_0(3^3P_0)$ | | 6.4517 | 3.7867 | 0.6 [36] | 0.02335 | 0.01670 |
| | $h_b(3^1P_1)$ | $\eta_b(1^1S_0)$ | 6.05386 | 7.4577 | 3.6 [20] | 0.014362 | 0.01225 |
| $3P \to 2D$ | $\chi_2(3^3P_2)$ | $\Upsilon_3(2^3D_3)$ | 2.7611 | 1.7238 | 1.5 [20] | 2.9803 | 2.2670 |
| | | $\Upsilon_2(2^3D_2)$ | 0.5294 | 0.4278 | 0.32 [20] | 0.5507 | 0.41735 |
| | | $\Upsilon(2^3D_1)$ | 0.03922 | 0.0422 | 0.027 [20] | 0.03897 | 0.02942 |
| | $\chi_1(3^3P_1)$ | $\Upsilon_2(2^3D_2)$ | 2.5888 | 1.2959 | 1.1 [20] | 2.7018 | 1.8188 |
| | | $\Upsilon(2^3D_1)$ | 0.959694 | 0.02735 | 0.4 [36] | 0.9565 | 0.6427 |
| | $\chi_0(3^3P_0)$ | $\Upsilon(2^3D_1)$ | 3.5427 | 1.2941 | 0.9 [36] | 3.5887 | 2.0013 |
| | $h_b(3^1P_1)$ | $\eta_{2b}(2^1D_2)$ | 3.2641 | 1.8727 | 1.6 [20] | 3.5555 | 2.5194 |
| $3P \to 1D$ | $\chi_2(3^3P_2)$ | $\Upsilon_3(1^3D_3)$ | 0.003086 | 0.00995 | 0.046 [20] | 0.01358 | 0.009085 |
| | | $\Upsilon_2(1^3D_2)$ | 0.0007225 | 0.002046 | ... | 0.00246 | 0.001625 |
| | | $\Upsilon_(1^3D_1)$ | 0.00005047 | 0.0001492 | 0 [36] | 0.000168 | 0.0001094 |
| | $\chi_1(3^3P_1)$ | $\Upsilon_2(1^3D_2)$ | 0.003593 | 0.009114 | 0.080 [20] | 0.01222 | 0.0077515 |
| | | $\Upsilon(1^3D_1)$ | 0.001255 | 0.0001334 | $7 \times 10^{-3}$ [36] | 0.00418 | 0.002611 |
| | $\chi_0(3^3P_0)$ | $\Upsilon(1^3D_1)$ | 0.004922 | 0.01129 | 0.2 [36] | 0.01636 | 0.009612 |
| | $h_b(3^1P_1)$ | $\eta_{2b}(1^1D_2)$ | 0.011687 | 0.01829 | 0.081 [20] | 0.01439 | 0.009124 |

of hybrid $b\bar{b}$ states show that these values are smaller as compared to the values for corresponding transitions for conventional states. These differences can be attributed to differences in the values of masses and radial wave functions.

Using our calculated masses and reported widths of conventional and hybrid mesons, we can identify the $\Upsilon(10860)$, $\Upsilon(11020)$, and $Y_b(10890)$ with help of the available experimental data.

### A. $\Upsilon(10860)$

$\Upsilon(10860)$ has mass $10891 \pm 4$ MeV, $J^{PC} = 1^{--}$, and leptonic decay width $0.31 \pm 0.07$ keV [38]. The comparison of its experimental mass with calculated values of $1^{--}$ states shows that $\Upsilon(10860)$ could be the $5S$ or $6S$ state of conventional bottomonium or the $h_b^h(1P)$ hybrid state. However, Table IV shows that the calculated value of the leptonic decay width of the $5S$ state (0.23 keV) is closer to the experimental value than that of the $6S$ state. Since the leptonic decay widths of hybrid states are generally much lower than the conventional states, $\Upsilon(10860)$ is unlikely to be a hybrid states. Thus, we suggest that $\Upsilon(10860)$ is the $5S$ state of conventional bottomonium. Reference [31] also assigns $\Upsilon(10860)$ as $5S$ while ignoring the relativistic corrections, which are quite significant for bottomonia. In this reference, the parameters of potential are fitted using $S$ states only, whereas we include ten bottomonium mesons with different $S$, $P$, and $D$ states. On the other hand, Ref. [27] assigns it $6S$ state using a potential which is screened at small distance by light $q\bar{q}$ pairs created in hadronic vacuum. However, that analysis is merely based on the comparison of mass values.

### B. $\Upsilon(11020)$

$\Upsilon(11020)$ has mass $10987.5^{+11}_{-3.4}$ MeV, $J^{PC} = 1^{--}$ and leptonic decay width $\Gamma_{ee} = 0.130 \pm 0.030$ keV [38]. The

TABLE IX. 1D and 2D, $E1$ radiative transitions.

| Transition | Initial meson | Final meson | Our calculated $\Gamma_{E1}$ | | Others theor. calculated $\Gamma_{E1}$ | Our calculated $\Gamma_{E1}$ for hybrid | |
|---|---|---|---|---|---|---|---|
| | | | NR [keV] | Relativistic [keV] | [20] [keV] | NR [keV] | Relativistic [keV] |
| $1D \to 1P$ | $\Upsilon_3(1^3D_3)$ | $\chi_2(1^3P_2)$ | 31.2721 | 37.4118 | 24.3 | 2.1424 | 1.3347 |
| | $\Upsilon_2(1^3D_2)$ | $\chi_2(1^3P_2)$ | 5.48044 | 8.0209 | 5.6 | 0.5108 | 0.3319 |
| | | $\chi_1(1^3P_1)$ | 21.025 | 29.9376 | 19.2 | 1.6137 | 1.0501 |
| | $\Upsilon(1^3D_1)$ | $\chi_2(1^3P_2)$ | 0.568022 | 0.8016 | 0.56 | 0.05196 | 0.0355 |
| | | $\chi_1(1^3P_1)$ | 10.9584 | 15.0785 | 9.7 | 0.8220 | 0.5621 |
| | | $\chi_0(1^3P_0)$ | 21.5026 | 28.5597 | 16.5 | 1.2419 | o.8539 |
| | $h_{b2}(1^1D_2)$ | $h_c(1^1P_1)$ | 25.8402 | 37.5565 | 24.9 | 2.1301 | 1.3757 |
| $2D \to 2P$ | $\Upsilon_3(2^3D_3)$ | $\chi_2(2^3P_2)$ | 5.066356 | 6.26455 | 16.4 | 2.9765 | 1.8549 |
| | $\Upsilon_2(2^3D_2)$ | $\chi_2(2^3P_2)$ | 1.20268 | 1.2878 | 3.8 | 0.7157 | 0.4466 |
| | | $\chi_1(2^3P_1)$ | 5.06132 | 5.4054 | 12.7 | 2.2132 | 1.4978 |
| | $\Upsilon(2^3D_1)$ | $\chi_2(2^3P_2)$ | 0.123364 | 0.1075 | 0.4 | 0.07410 | 0.04621 |
| | | $\chi_1(2^3P_1)$ | 2.61871 | 2.3302 | 6.5 | 1.1466 | 0.07770 |
| | | $\chi_0(2^3P_0)$ | 5.87955 | 5.3734 | 10.6 | 1.6822 | 1.2922 |
| | $\eta_{b2}(2^1D_2)$ | $h_c(2^1P_1)$ | 13.7231 | 11.658 | 16.5 | 2.9664 | 1.9484 |
| $2D \to 1P$ | $\Upsilon_3(2^3D_3)$ | $\chi_2(1^3P_2)$ | 2.90251 | 3.9918 | 2.6 | 0.03892 | 0.0460 |
| | $\Upsilon_2(2^3D_2)$ | $\chi_2(1^3P_2)$ | 0.717137 | 0.9530 | 0.4 | 0.00961 | 0.01137 |
| | | $\chi_1(1^3P_1)$ | 2.42052 | 3.2158 | 2.6 | 0.02930 | 0.0347 |
| | $\Upsilon(2^3D_1)$ | $\chi_2(1^3P_2)$ | 0.0782558 | 0.09939 | 0.02 | 0.001046 | 0.001238 |
| | | $\chi_1(1^3P_1)$ | 1.32166 | 1.6815 | 0.9 | 0.01594 | 0.01887 |
| | | $\chi_0(1^3P_0)$ | 2.13601 | 2.7245 | 2.9 | 0.02208 | 0.02628 |
| | $h_{b2}(2^1D_2)$ | $h_c(1^1P_1)$ | 3.31247 | 4.3669 | 3 | 0.03686 | 0.04394 |
| $2D \to 1F$ | $\Upsilon_3(2^3D_3)$ | $\chi_4(1^3F_4)$ | 1.5356 | 1.1737 | 1.7 | 1.5441 | 1.1421 |
| | | $\chi_3(1^3F_3)$ | | 0.1113 | 0.16 | 0.1365 | 0.09658 |
| | | $\chi_2(1^3F_2)$ | | 0.003629 | $5 \times 10^{-3}$ | 0.00409 | 0.002759 |
| | $\Upsilon_2(2^3D_2)$ | $\chi_3(1^3F_3)$ | 1.56236 | 0.9104 | 1.5 | 1.4778 | 0.9903 |
| | | $\chi_2(1^3F_2)$ | | 0.13177 | 0.21 | 0.1939 | 0.1311 |
| | $\Upsilon(2^3D_1)$ | $\chi_2(1^3F_2)$ | | 0.7497 | 1.6 | 1.6439 | 1.1141 |
| | $\eta_{b2}(2^1D_2)$ | $h_{c3}(1^1F_3)$ | 1.73254 | 1.0752 | 1.8 | 1.6696 | 1.19693 |

comparison of its experimental mass and $J^{PC}$ with our results implies that it could be the $6S$ state of conventional bottomonim or $2P$ hybrid state or $3P$ hybrid state. However, the possibility of this being hybrid is unlikely as the measured decay width is higher than that expected for the hybrids. As given in Table IV, the calculated value of $\Gamma_{ee}$ for the $6S$ state is 0.20 keV, assuming the relativistic correction term $\Delta(nS) = 0.20$ (estimated from the experiment value of $\Gamma_{ee}$ of the $4S$ state). As remarked earlier, the value of $\Delta(nS)$ is state dependent and expected to be small for higher excited states. If this correction term is ignored for the $6S$ state, then calculated $\Gamma_{ee}$ reduces to 0.128 keV, which is very close to the experimental value. References [22,31] also assign $\Upsilon(11020)$ as the $6S$ state of the bottomonium meson, contrary to Ref. [27]. This reference assigns $\Upsilon(11020)$ to the $7S$ state along with $\Upsilon(10860)$ to the $6S$ state by considering the $5S$ state as yet undiscovered.

### C. $Y_b(10890)$

$Y_b(10890)$ has mass $10888.4 \pm 3$ MeV [39], $J^{PC} = 1^{--}$, and the leptonic decay width is not yet measured. The measured value of mass in this case closely corresponds to the $5S$ state of the conventional bottomonium and the $1P$ hybrid state, both having $J^{PC} = 1^{--}$. Since we have the $5S$ state assigned to $\Upsilon(10860)$, we suggest that $Y_b(10890)$ could be the $1P$ hybrid state. Reference [29] also suggests that $Y_b(10890)$ is a candidate for the bottomonium hybrid $1^{--}$ state, and its decay to the $\Upsilon$ suggests that $Y_b(10890)$ is not a conventional bottomonium meson as this decay violates the spin symmetry. In Refs. [40,41], the estimated mass of the $1^{--}$ bottomonium

TABLE X. 1F and 2F, $E1$ radiative transitions.

| Transition | Initial meson | Final meson | Our calculated $\Gamma_{E1}$ NR [keV] | Our calculated $\Gamma_{E1}$ Relativistic [keV] | Others theor. calculated $\Gamma_{E1}$ [20] [keV] | Our calculated $\Gamma_{E1}$ for hybrid keV [NR] | Our calculated $\Gamma_{E1}$ for hybrid Relativistic [keV] |
|---|---|---|---|---|---|---|---|
| $1F \to 1D$ | $\chi_4(1^3F_4)$ | $\Upsilon_3(1^3D_3)$ | 9.5648 | 10.9949 | 18 | 3.50637 | 2.2932 |
| | $\chi_3(1^3F_3)$ | $\Upsilon_3(1^3D_3)$ | 0.986547 | 1.1616 | 1.9 | 0.3801 | 0.2612 |
| | | $\Upsilon_2(1^3D_2)$ | 14.2317 | 12.348 | 16.7 | 3.1809 | 2.1002 |
| | $\chi_2(1^3F_2)$ | $\Upsilon_3(1^3D_3)$ | 0.0357111 | 0.0430 | 0.07 | 0.01441 | 0.0104 |
| | | $\Upsilon_2(1^3D_2)$ | 2.2958 | 2.01672 | 2.7 | 0.5278 | 0.3675 |
| | | $\Upsilon(1^3D_1)$ | 13.676 | 13.004 | 16.4 | 3.09214 | 2.0543 |
| | $h_{b3}(1^1F_3)$ | $\eta_{c2}(1^1D_2)$ | 15.9777 | 13.2407 | 18.8 | 3.5635 | 2.3504 |
| $2F \to 2D$ | $\chi_4(2^3F_4)$ | $\Upsilon_3(2^3D_3)$ | 14.0995 | 10.4506 | 19.6 | 4.2665 | 2.7635 |
| | $\chi_3(2^3F_3)$ | $\Upsilon_3(2^3D_3)$ | 1.50403 | 1.07438 | 2.1 | 0.46022 | 0.3086 |
| | | $\Upsilon_2(2^3D_2)$ | 12.561 | 10.3987 | 17.9 | 3.8245 | 2.559 |
| | $\chi_2(2^3F_2)$ | $\Upsilon_3(2^3D_3)$ | 0.0565314 | 0.03851 | 0.08 | 0.01749 | 0.01215 |
| | | $\Upsilon_2(2^3D_2)$ | 2.06744 | 1.6423 | 3 | 0.6361 | 0.4410 |
| | | $\Upsilon(2^3D_1)$ | 11.9235 | 11.3486 | 17.5 | 3.6751 | 2.5432 |
| | $h_{b3}(2^1F_3)$ | $\eta_{c2}(2^1D_2)$ | 14.1418 | 11.3816 | 19.9 | 4.2826 | 2.8476 |
| $2F \to 1D$ | $\chi_4(2^3F_4)$ | $\Upsilon_3(1^3D_3)$ | 1.05143 | 1.1283 | 1.4 | 0.008949 | 0.01506 |
| | $\chi_3(2^3F_3)$ | $\Upsilon_3(1^3D_3)$ | 0.115071 | 0.1220 | $2 \times 10^{-3}$ | 0.000985 | 0.001676 |
| | | $\Upsilon_2(1^3D_2)$ | 1.15993 | 1.1003 | | 0.007997 | 0.01343 |
| | $\chi_2(2^3F_2)$ | $\Upsilon_3(1^3D_3)$ | 0.00449888 | 0.004701 | 0.1 | 0.00003878 | 0.00006671 |
| | | $\Upsilon_2(1^3D_2)$ | 0.198759 | 0.1858 | 1.4 | 0.001377 | 0.002339 |
| | | $\Upsilon(1^3D_1)$ | 1.11751 | 1.0837 | 1.6 | 0.007637 | 0.01277 |
| | $h_{b3}(2^1F_3)$ | $\eta_{c2}(1^1D_2)$ | 1.32504 | 1.2458 | 1.6 | 0.008846 | 0.01485 |

TABLE XI. $M1$ radiative transitions calculated by taking the experimental masses from the Particle Data Group [21].

| Transition | Initial meson | Final meson | Our calculated $\Gamma_{M1}$ NR [keV] | Our calculated $\Gamma_{M1}$ Relativistic [keV] | Exp. calculated $\Gamma_{M1}$ keV | Others theor. calculated $\Gamma_{M1}$ [20] [keV] | Our calculated $\Gamma_{M1}$ for hybrid NR [keV] | Our calculated $\Gamma_{M1}$ for hybrid Relativistic [keV] |
|---|---|---|---|---|---|---|---|---|
| $1S$ | $\Upsilon(1^3S_1)$ | $\eta_b(1^1S_0)$ | 0.0110347 | 0.0002302 | | 0.010 | $1.01993 \times 10^{-7}$ | $4.5204 \times 10^{-8}$ |
| 2S | $\Upsilon(2^3S_1)$ | $\acute{\eta}_b(2^1S_0)$ | 0.0006584 | 0.00004591 | | $5.9 \times 10^{-4}$ | $6.4135 \times 10^{-7}$ | $2.6351 \times 10^{-7}$ |
| | | $\eta_b(1^1S_0)$ | 0.01729 | 0.0008832 | $0.012 \pm 0.004$ | 0.081 | 0.000022269 | $9.3836 \times 10^{-6}$ |
| | $\eta_b(2^1S_0)$ | $\Upsilon(1^3S_1)$ | 0.0006363 | 0.003021 | | 0.068 | 0.0002045 | 0.00002694 |
| 3S | $\Upsilon(3^3S_1)$ | $\eta_b(3^1S_0)$ | 0.011914 | 0.01948 | | $2.5 \times 10^{-4}$ | $1.01803 \times 10^{-6}$ | $4.1833 \times 10^{-7}$ |
| | | $\eta_b(2^1S_0)$ | 0.0030422 | 0.000151 | $<0.12$ | 0.19 | 0.00004661 | 0.00001922 |
| | | $\eta_b(1^1S_0)$ | 0.01718 | 0.0007183 | $0.01 \pm 0.002$ | 0.060 | 0.00004924 | 0.0000196 |
| | $\eta_b(3^1S_0)$ | $\acute{\Upsilon}(2^3S_1)$ | 0.0000107 | 0.0001993 | $0.949 \pm 0.098$ | 0.95 | 0.00013129 | 0.00005409 |
| | | $J/\Upsilon(1^3S_1)$ | 0.000116988 | 0.001816 | $1.335 \pm 0.125$ | 1.34 | 0.0001390 | 0.00005519 |
| 2 P | $h_b(2^1P_1)$ | $\chi_2(1^3P_2)$ | 0.0002621 | 0.0001772 | | $2.2 \times 10^{-3}$ | $4.1391 \times 10^{-7}$ | $3.6028 \times 10^{-7}$ |
| | | $\chi_1(1^3P_1)$ | 0.0002684 | 0.0001261 | | $1.1 \times 10^{-3}$ | $2.5419 \times 10^{-7}$ | $2.2125 \times 10^{-7}$ |
| | | $\chi_0(1^3P_0)$ | 0.000198333 | 0.00005515 | | $3.2 \times 10^{-4}$ | $8.9566 \times 10^{-8}$ | $7.8111 \times 10^{-8}$ |
| | $\chi_2(2^3P_2)$ | $h_b(1^1P_1)$ | 0.001620 | 0.0001566 | | $2.4 \times 10^{-4}$ | $2.5471 \times 10^{-7}$ | $2.26827 \times 10^{-7}$ |
| | $\chi_1(2^3P_1)$ | $h_b(1^1P_1)$ | 0.001323 | 0.0001409 | | $2.2 \times 10^{-3}$ | $2.5129 \times 10^{-7}$ | $2.1607 \times 10^{-7}$ |
| | $\chi_0(2^3P_0)$ | $h_b(1^1P_1)$ | 0.0009181 | 0.000116 | | $9.7 \times 10^{-3}$ | $2.4075 \times 10^{-7}$ | $1.9511 \times 10^{-7}$ |

hybrid is compatible to the mass of $Y_b(10890)$. However, Refs. [42] are in favor of $Y_b(10890)$ being a tetraquark.

## IV. SUMMARY

We show that our lattice-based extension of the quark potential model to gluonic excitations allows us to conveniently calculate the properties of both the conventional and hybrid bottomonium mesons without and with orbital and radial excitations. All this is needed to actively take part in the discussion for recognizing mesons in this sector. Relativistic corrections are included in our work. We find additional evidence to support the recent suggestion of assigning $Y_b(10890)$ to be the $1P$ hybrid state. Our calculated conventional and hybrid masses and leptonic widths indicate that $\Upsilon(10860)$ and $\Upsilon(11020)$ are $5S$ and $6S$ states of bottomonium mesons. We find how much hybrid meson masses and radii are more than those of the conventional mesons for the same $n$, $L$, and $S$ quantum numbers. Because of smaller values of the radial wave functions at the origin for hybrids as compared to conventional meson states, our leptonic and photonic decay widths of hybrid states are much smaller than the conventional states. It is also observed that, in contrast to the trend for the conventional mesons, hybrid decay rates increase with the principal quantum number. These can be useful signatures for recognizing hybrid mesons. Our values of $M1$ and $E1$ radiative transition for conventional bottomonium mesons have good agreement with the corresponding experimental data. We find that for hybrid $b\bar{b}$ states the values of the radiative decay widths are generally smaller than for conventional states. Given that the masses of hybrids states are always greater than the $B\bar{B}$ threshold, we require high statistics to detect any signal for hybrids states notable through radiative transitions in present and future B factories.

Overall, this implementation indicates that our extended potential model can be used to advance predictions in a variety of meson sectors.

## ACKNOWLEDGMENTS

B. M. and F. A. acknowledge the financial support of Punjab University for Sr. 20 PU Project 2014-15 and Sr. 21 PU Project 2014-15. N. A. is grateful to Higher Education Commission of Pakistan for their financial support (Grant No. PM-IPFP/HRD/HEC/2014/1703).

[1] N. Akbar, B. Masud, and S. Noor, Eur. Phys. J. A **47**, 124 (2011); **50**, 121(E) (2014).
[2] K. J. Juge, J. Kuti, and C. Morningstar, AIP Conf. Proc. **688**, 193 (2003).
[3] A. Sultan, N. Akbar, B. Masud, and F. Akram, Phys. Rev. D **90**, 054001 (2014).
[4] N. Isgur and J. Paton, Phys. Rev. D **31**, 2910 (1985).
[5] K. J. Juge, J. Kuti, and C. J. Morningstar, Phys. Rev. Lett. **82**, 4400 (1999).
[6] E. Braaten, C. Langmack, and D. H. Smith, Phys. Rev. D **90**, 014044 (2014).
[7] F. Iddir and L. Semlala, Int. J. Mod. Phys. A **23**, 5229 (2008).
[8] F. Iddir and L. Semlala, arXiv:hep-ph/0611165.
[9] F. Iddir and L. Semlala, arXiv:hep-ph/0611183.
[10] R. Berg, D. Harnett, R. T. Kleiv, and T. G. Steele, Phys. Rev. D **86**, 034002 (2012).
[11] D. Harnett, R. Berg, R. T. Kleiv, and T. G. Steele, Nucl. Phys. B, Proc. Suppl. **234**, 154 (2013).
[12] D. Harnett, R. T. Kleiv, T. G. Steele, and H. y. Jin, J. Phys. G **39**, 125003 (2012).
[13] R. T. Kleiv, D. Harnett, T. G. Steele, and H. y. Jin, Nucl. Phys. B, Proc. Suppl. **234**, 150 (2013).
[14] R. T. Kleiv, B. Bulthuis, D. Harnett, T. Richards, W. Chen, J. Ho, T. G. Steele, and S.-L. Zhu, Can. J. Phys. **93**, 952 (2015).
[15] W. Chen, J. Ho, T. G. Steele, R. T. Kleiv, B. Bulthuis, D. Harnett, T. Richards, and S.-L. Zhu, *Proceedings of the 30th International Workshop on High Energy Physics: Particle and Astroparticle Physics, Gravitation and Cosmology: Predictions, Observations and New Projects (IHEP 2014), Protvino, Russia, 2014*, edited by V. A. Petrov, R. A. Ryutin (unpublished).
[16] C. F. Qiaoa, L. Tang, G. Hao, and X.-Q. Li, J. Phys. G **39**, 015005 (2012).
[17] W. Chen, T. G. Steele, and S.-L. Zhu, The Universe **2**, 1 (2014).
[18] J. Y. Cui, H. Y. Jin, and J. M. Wu, Int. J. Mod. Phys. A **14**, 2273 (1999).
[19] T. Barnes, S. Godfrey, and E. S. Swanson, Phys. Rev. D **72**, 054026 (2005).
[20] S. Godfrey and K. Moats, Phys. Rev. D **92**, 054034 (2015).
[21] K. A. Olive *et al.* (Particle Data Group Collaboration), Chin. Phys. C **38**, 090001 (2014).
[22] B.-Q. Li and K.-T. Chao, Commun. Theor. Phys. **52**, 653 (2009).
[23] O. Lakhina and E. S. Swanson, Phys. Rev. D **74**, 014012 (2006).
[24] T. Branz, T. Gutsche, V. E. Lyubovitskij, I. Schmidt, and A. Vega, Phys. Rev. D **82**, 074022 (2010).
[25] C. J. Morningstar and M. Peardon, Phys. Rev. D **60**, 034509 (1999).
[26] K. J. Juge, J. Kuti, and C. J. Morningstar, Phys. Rev. Lett. **82**, 4400 (1999).
[27] P. Gonzalez, Phys. Rev. D **80**, 054010 (2009).

[28] F. E. Close and J. J. Dudek, Phys. Rev. D **69**, 034010 (2004); Phys. Rev. Lett. **91**, 14 (2001).
[29] M. Berwein, N. Brambilla, J. T. Castella, and A. Vairo, Phys. Rev. D **92**, 114019 (2015).
[30] Wei Chen, R. T. Kleiv, T. G. Steele, B. Bulthuis, D. Harnett, J. Ho, T. Richards, and S.-L. Zhu, J. High Energy Phys. 09 (2013) 019.
[31] J. Segovia, D. R. Entem, and F. Fernandez, Phys. Rev. D **91**, 014002 (2015).
[32] H.-W. Ke, J. Tang, X.-Q. Hao, and X.-Q. Li, Phys. Rev. D **76**, 074035 (2007).
[33] K. Han *et al.*, Phys. Rev. Lett. **49**, 1612 (1982); G. Eigen *et al.*, Phys. Rev. Lett. **49**, 1616 (1982); C. Klopfenstein *et al.* (CUSB Collaboration), Phys. Rev. Lett. **51**, 160 (1983); M. Artuso *et al.* (CLEO Collaboration), Phys. Rev. Lett. **94**, 032001 (2005).
[34] ATLAS Collaboration, Phys. Rev. Lett. **108**, 152001 (2012).
[35] A. Grant and J. L. Rosner, Phys. Rev. D **46**, 3862 (1992).
[36] J. Ferretti, Eur. Phys. J. Web Conf. **96**, 01012 (2015).
[37] J. Beringer *et al.* (Particle Data Group Collaboration), Phys. Rev. D **86**, 010001 (2012).
[38] C. Patrignani *et al.* (Particle Data Group Collaboration), Chin. Phys. C **40**, 100001 (2016).
[39] K. F. Chen *et al.* (Belle Collaboration), Phys. Rev. D **82**, 091106 (2010).
[40] C.-F. Qiao, L. Tang, G. Hao, and X.-Q. Li, J. Phys. G **39**, 015005 (2012).
[41] C. Semay, F. Buisseret, and B. Silvestre-Brac, Phys. Rev. D **79**, 094020 (2009).
[42] A. Ali, C. Hambrock, and M. J. Aslam, Phys. Lett. B **684**, 28 (2010).